Supporting Information

# Significantly enhanced high-temperature capacitive energy storage in cyclic olefin copolymer dielectric films via ultraviolet irradiation

Zhiwei Bao,[a] Song Ding,[a] Zhizhan Dai,[a] Yiwei Wang,[a] Jiangheng Jia,[a] Shengchun Shen,[a] Yuewei Yin[*a] and Xiaoguang Li[*ab]

Table of Contents

─────────────────

*a Hefei National Research Center for Physical Sciences at the Microscale, Department of Physics, and CAS Key Laboratory of Strongly-coupled Quantum Matter Physics, University of Science and Technology of China, Hefei 230026, China*

*E-mail: lixg@ustc.edu.cn, yyw@ustc.edu.cn*

*b Collaborative Innovation Center of Advanced Microstructures, Nanjing University, Nanjing 210093, China*
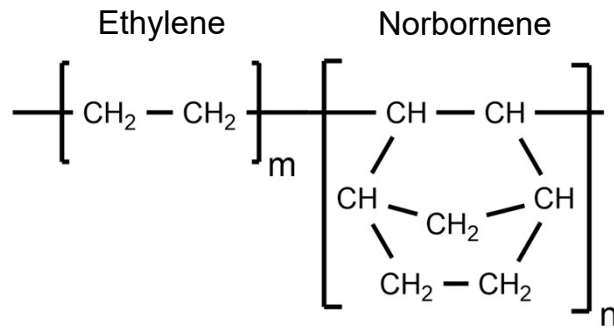
## 1. Chemical structure of COC



**Fig. S1** Chemical structure of COC

The cyclic olefin copolymer (COC) is composed of ethylene and ring-shaped norbornene groups, as shown in Fig. S1. Norbornene is much bulkier than ethylene and has a rigid saturated bicyclic structure.[1,2] Generally, polymers with this rigid structure as the backbone will have a high glass transition temperature ($T_g$).[3,4] The norbornene content in COC-6017S-04 is approximately 83 wt% with a high $T_g$ value of ~178 °C.[5,6] The high $T_g$ of polymers is beneficial to the high-temperature dielectric stability.[7]

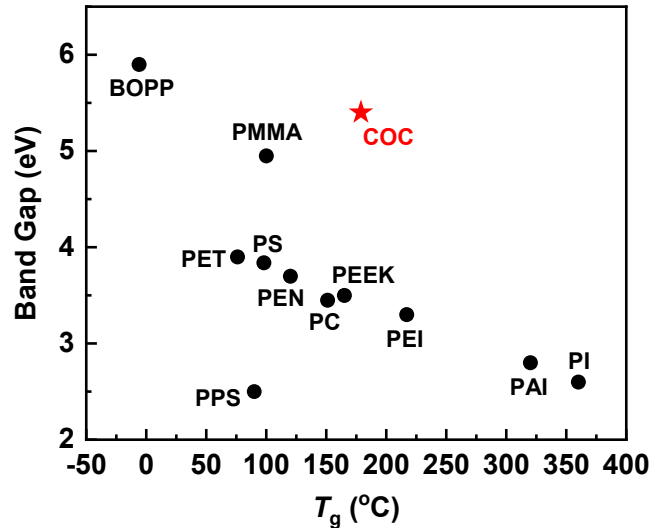## 2. Band gap versus $T_g$ for various commercial dielectric polymers



**Fig. S2** Band gap versus $T_g$ for various representative commercial dielectric polymers.

For dielectrics, the band gap is an important parameter for determining the electric field endurance. Due to the fully saturated σ-bonding in the main chains, COC-6017S-04 has a large bandgap (~5.40 eV).[8,9] A material with a wide bandgap makes it difficult for electrons to jump between the bandgap, and this is advantageous for obtaining higher insulation, which is beneficial for the energy storage performance of dielectrics.[1,4,10] Generally, the larger the band

gap is, the higher the breakdown strength ($E_b$).[11-13] $T_g$ is an established gauge parameter for polymer thermal stability. To operate at high temperature, polymers with high $T_g$ are necessary because they may lose their mechanical integrity when the operation temperature is close to $T_g$.[3] Above $T_g$, the drastically enhanced segmental motion of polymer chains may give rise to significantly increased leakage current and conduction loss, leading to a poor energy storage performance, such as a low efficiency, etc.[1,14] However, polymers with high $T_g$ usually contain lots of benzene rings, which would form π-π conjugates and reduce the band gap ($E_g$) of polymers,[9,15] leading to increased leakage at high electric fields and high temperatures.[15,16] Thus, the band gap and $T_g$ typically show an inverse relationship. For example, as shown in Fig. S2, biaxially oriented polypropylene (BOPP), the state-of-the-art commercial polymer dielectric, displays the largest band gap of ~5.9 eV.[3] However, it can only work below 105 °C owing to the low $T_g$ of ~ -6 °C.[17] Polyimide (PI) exhibits the highest $T_g$ of ~360 °C while with a band gap as low as ~2.6 eV. Fortunately, COC-6017S-04 has a wide band gap of ~5.4 eV and a relatively high $T_g$ of ~178 °C simultaneously,[9,18] making it an outlier compared to other representative commercial dielectric polymers.[3,19-27]

## 3. Cross-sectional morphologies

The cross-sectional images of irradiated COC-6017S-04 films are shown in Fig. S3. It can be seen that the thicknesses of the films are approximately 12 ± 2 μm. All the films fabricated by solution-casting method exhibit compact and dense microstructure, demonstrating the high quality of our films.
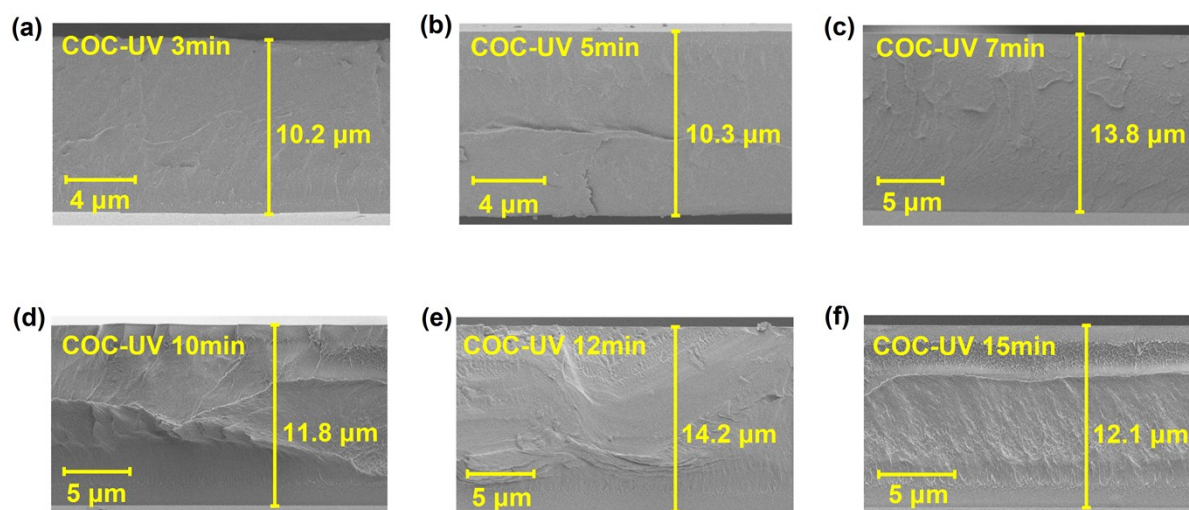


**Fig. S3** Cross-sectional SEM images of COC-6017S-04 films with different irradiation durations of (a) 3 min, (b) 5 min, (c) 7 min, (d) 10 min, (e) 12 min and (f) 15 min.

## 4. Thermogravimetric analysis (TGA) curves

Thermal stability is very important for the polymer to work at high temperatures. Thus, the thermogravimetric analysis (TGA) curves of pristine and irradiated COC-6017S-04 films were measured, as shown in Fig. S4a. 10% weight loss temperature ($T_{10\%}$) is an important parameter to evaluate the thermal stability of materials,[28-30] and the $T_{10\%}$ values of COC-6017S-04 films under different ultraviolet (UV) irradiation conditions are shown in Fig. S4b. The $T_{10\%}$ of pristine COC-6017S-04 film is ~445.8 °C. After UV irradiation, the $T_{10\%}$s of irradiated films decrease monotonically with increasing irradiation time. For example, the $T_{10\%}$ of COC-UV 10min film drops to ~432.1 °C. The chain scission of polymer under UV irradiation may account for the degenerated thermal stability, similar to the earlier reports on poly(L-lactide) (PLLA), poly(ether ether ketone) (PEEK), and ethylene-vinyl acetate copolymer (EVA), etc.[31-33] In spite of this, it is worth noting that even for the COC-UV 15min, the $T_{10\%}$ is still as high as ~429.2 °C, much higher than the testing temperature of ~150 °C. These results strongly demonstrate that the COC-6017S-04 films have excellent thermal stability.
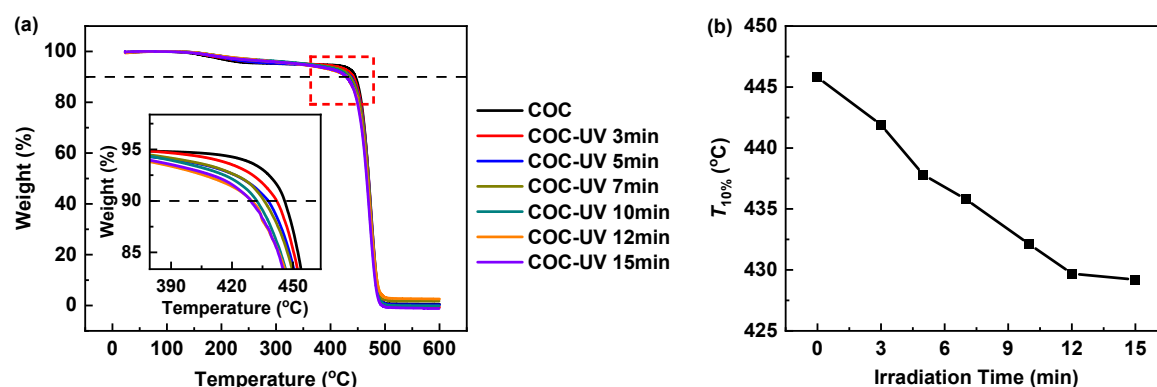


**Fig. S4** (a) TGA curves of pristine and irradiated COC-6017S-04 films. The inset image is the enlarged view from the dashed box. (b) Plot of $T_{10\%}$s of COC-6017S-04 films with different irradiation durations.

## 5. Dielectric properties at different temperatures

The dielectric spectra of pristine and irradiated COC-6017S-04 films from 1 kHz to 1 MHz at different temperatures from 20 °C to 150 °C are shown in Fig. S5. As the temperature increases, the dielectric constants of films decrease due to the increased thermal oscillation of molecules and the enhanced degree of disorder of dipoles at high temperatures.[34,35] Because of the nonpolar nature of COC-6017S-04,[36,37] the dielectric loss of all the films remains extremely low (below 0.004 at 1 kHz) from 20 °C to 150 °C.
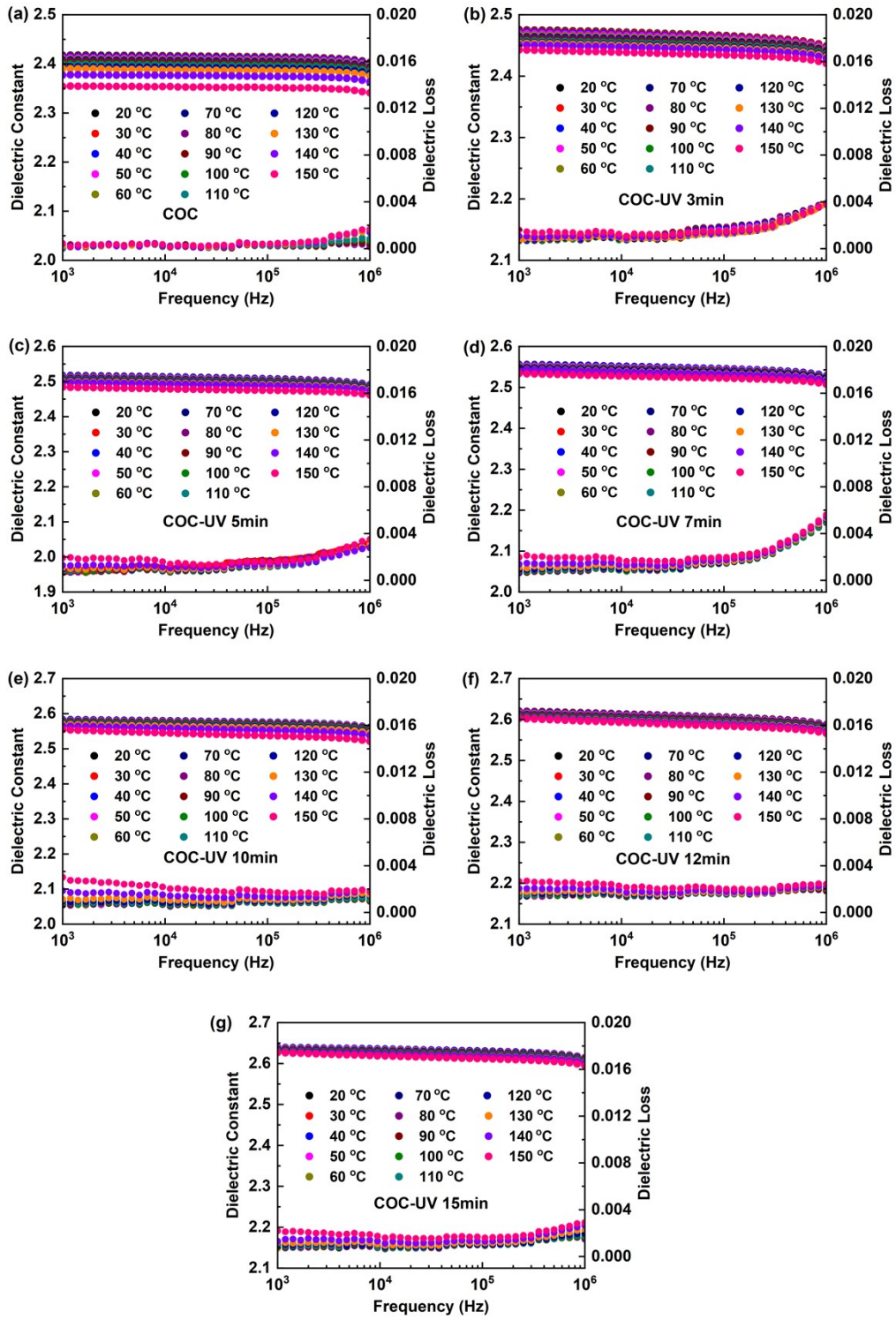
**Fig. S5** Dielectric spectra of (a) pristine COC-6017S-04 film and films irradiated with UV irradiation durations of (b) 3 min, (c) 5 min, (d) 7 min, (e) 10 min, (f) 12 min and (g) 15 min at different temperatures.

## 6. Unipolar displacement-electric field (*D-E*) loops at 150 °C

Fig. S6 shows *D-E* curves until the breakdown electric fields of pristine and irradiated COC-6017S-04 films. All the films show a typical dielectric behavior with linear and slim *D-*

*E* curves even at a high temperature of 150 °C. Benefitting from the enhanced dielectric constant and breakdown strength, the electric displacement of the COC-UV 10min film is ~1.62 $\mu C$ $cm^{-2}$, 35% higher than that of the pristine film (~1.20 $\mu C$ $cm^{-2}$). The increased electric displacement is beneficial for improving the capacitive energy density.



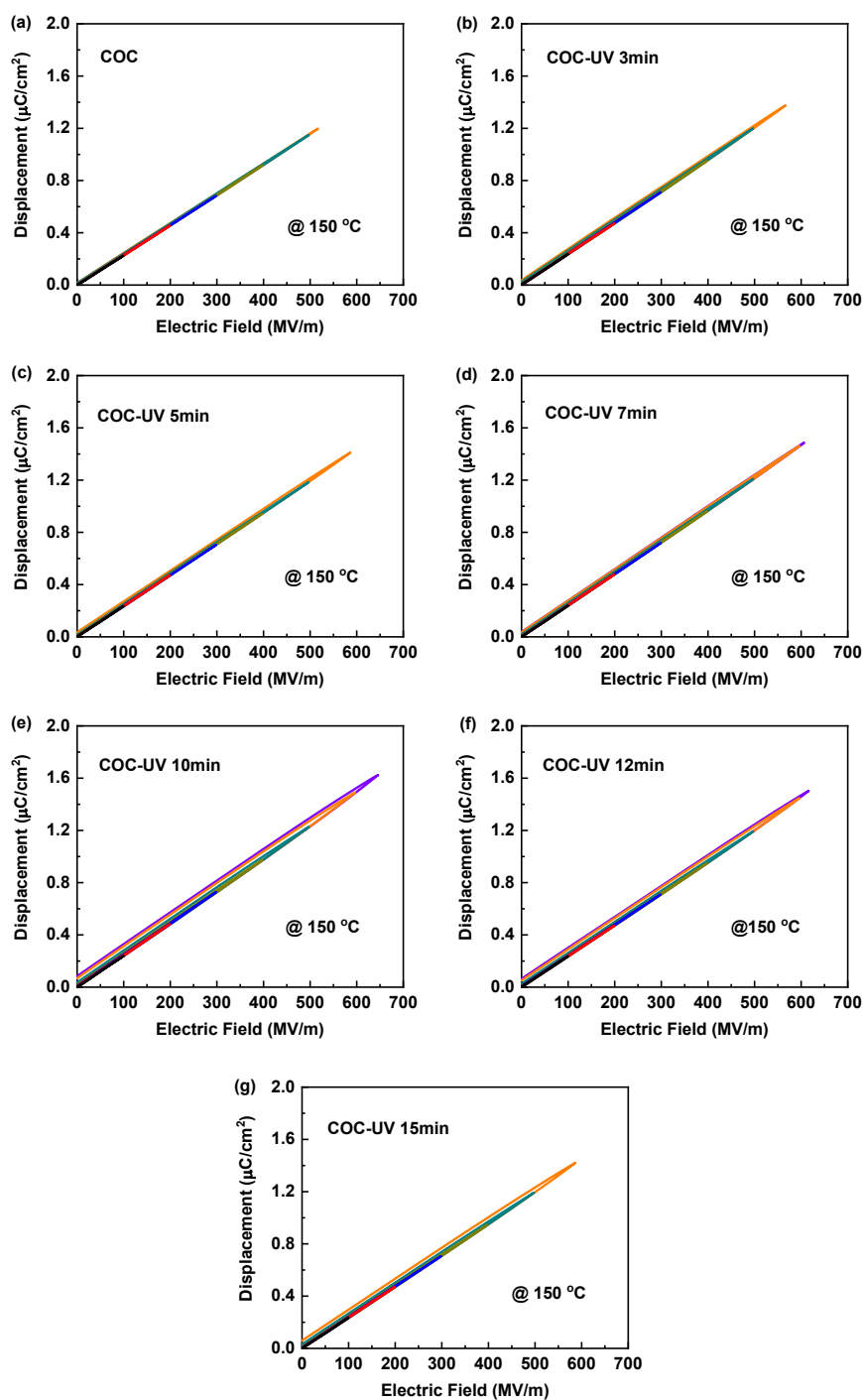**Fig. S6** *D-E* curves of (a) pristine COC-6017S-04 film and irradiated films with different UV irradiation durations of (b) 3 min, (c) 5 min, (d) 7 min, (e) 10 min, (f) 12 min and (g) 15 min under varied electric fields at 150 °C.

## 7. Dielectric energy storage performance

**Table S1.** The breakdown strength ($E_b$), discharged energy density ($U_e$), and energy storage efficiency ($\eta$) of pristine and irradiated COC-6017S-04 films at 150 °C.

| Samples | $E_b$ (MV m$^{-1}$) | $U_e$ (J cm$^{-3}$) | $\eta$ @ $E_b$ |
|---|---|---|---|
| COC | 520.8 | 3.07 | 97.5% |
| COC-UV 3min | 568.3 | 3.73 | 95.4% |
| COC-UV 5min | 583.3 | 4.00 | 95.3% |
| COC-UV 7min | 609.1 | 4.42 | 95.2% |
| COC-UV 10min | 644.8 | 5.18 | 92.2% |
| COC-UV 12min | 612.6 | 4.45 | 92.1% |
| COC-UV 15min | 582.1 | 4.06 | 91.9% |

Table S1 summarizes the dielectric energy storage performance, including breakdown strengths, discharged energy densities, and energy storage efficiencies at 150 °C. The COC-UV 10min film exhibits the maximum $E_b$ of 644.8 MV m$^{-1}$, 23.8% higher than that ~520.8 MV m$^{-1}$ of the pristine COC-6017S-04 films. Due to the maximum $E_b$ and increased $\varepsilon_r$, the discharged energy density of the COC-UV 10min film is ~5.18 J cm$^{-3}$, ~68.7% higher than ~3.07 J cm$^{-3}$ for the pristine film. Of particular importance is that the largely enhanced $E_b$ is not at the cost of the energy storage efficiency. For example, for the COC-UV 10min film, $\eta$ still maintains a high level of 92.2% at $E_b$.

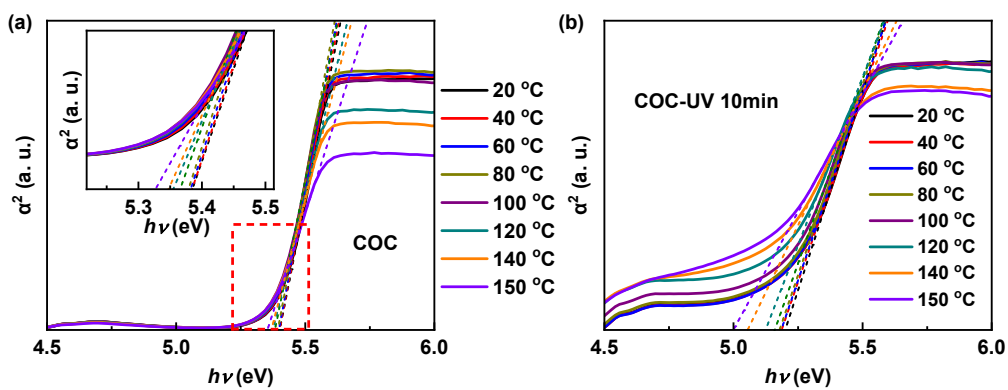## 8. Band gaps of films at different temperatures



**Fig. S7** Band gaps of pristine COC-6017S-04 film (a) and COC-UV 10min film (b) derived from UV-Visible spectroscopy.

The optical band gaps ($E_g$) of COC-6017S-04 and COC-UV 10min films are estimated from the ultraviolet absorption spectra following the equation:[38] $\alpha = A(h\nu - E_g)^{1/2}$. Here, $\alpha$, $A$,

*h and ν* stand for the optical absorption coefficient, proportional constant, Planck's constant and frequency of the incident photon, respectively. The plots of $\alpha^2$ against $h\nu$ for COC-6017S-04 and COC-UV 10min are plotted in Fig. S7a and Fig. S7b, respectively, and the band gaps were obtained by extrapolating the straight dotted line to the $h\nu$ axis.

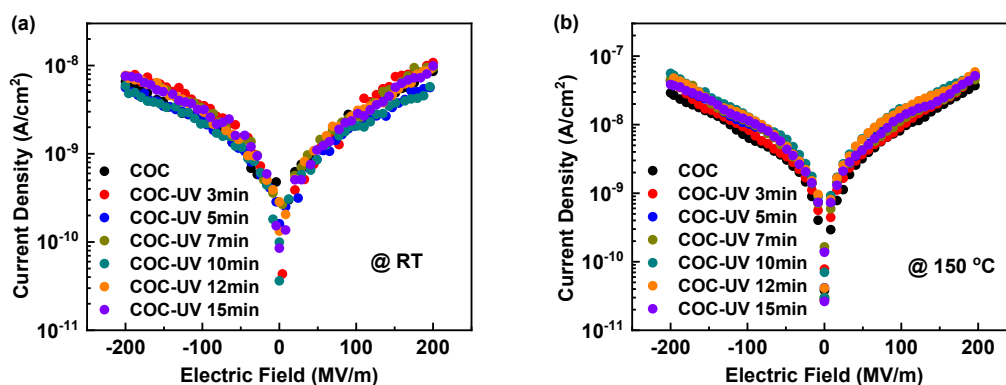## 9. Leakage current density at RT and 150 °C



**Fig. S8** Current densities of pristine and irradiated COC-6017S-04 films as a function of electric field at (a) RT and (b) 150 °C.

Fig. S8 shows the leakage currents of pristine and treated films at RT and 150 °C under 200 MV m$^{-1}$. It can be seen that the leakage current densities of all the films are low ($\sim 5.63 \times 10^{-9}$ A cm$^{-2}$ – $1.08 \times 10^{-8}$ A cm$^{-2}$) under 200 MV m$^{-1}$ at RT (Fig. S8a). When the temperature increases to 150 °C (Fig. S8b), the films still maintain a very low level ($\sim 3.71 \times 10^{-8}$ A cm$^{-2}$ – $5.89 \times 10^{-8}$ A cm$^{-2}$) under 200 MV m$^{-1}$. Such a low leakage current density is beneficial to avoid electrothermal breakdown.[39,40]

## 10. Energy storage performance of COC-6013 films

To verify the generality of our strategy for COC with different contents of norbornene, we investigated the effect of UV irradiation on the energy storage performance of COC-6013 film with a content of norbornene of $\sim$76 wt%.[41] Considering that the $T_g$ of COC-6013 is lower than 150 °C, we tested its energy storage performance at 125 °C. COC-6013 film was also prepared by solution casting, and the irradiation time for both sides of the COC-6013 film was set as 0, 1, 3, 7, and 10 min (labeled UV-0min, UV-1min, UV-3min, UV-7min, and UV-10min, respectively).

Fig. S9a shows Weibull distributions of breakdown strengths of pristine and irradiated COC-6013 films at 125°C. It can be seen that the breakdown strength ($E_b$) of COC-6013 film can also be improved by proper UV irradiation. For example, the $E_b$ of UV-7min film is 647.9 MV m$^{-1}$, which is $\sim$13.2% higher than $\sim$572.5 MV m$^{-1}$ of the pristine UV-0min film. With

further increasing the irradiation time to 10 min, the $E_b$ of UV-10min film decreases to ~643.6 MV m$^{-1}$. As discussed in the manuscript, the cross-linking and chain scission during UV irradiation play a key role in improving the $E_b$ of COC-6017S-04 film owing to the formation of polar carbonyl groups as well as broken bonds, which might generate deep traps and limit charge transport.[42-44] Similarly, for COC-6013, when the irradiation time is ≤7 min, the $E_b$s are enhanced because of the cross-linking and chain scission. While with further increasing irradiation time, the decrease of $E_b$s might be related to the possible degradation by excessive UV irradiation.[42,43,45,46]

The electric displacement-electric field (*D-E*) curves of the pristine and irradiated COC-6013 films are shown in Fig. S9b, and even at 125 °C, all the films exhibit standard linear dielectric characteristics. The discharged energy density ($U_e$) and energy storage efficiency ($\eta$) as a function of electric field are shown in Fig. S9c and Fig. S9d, respectively.



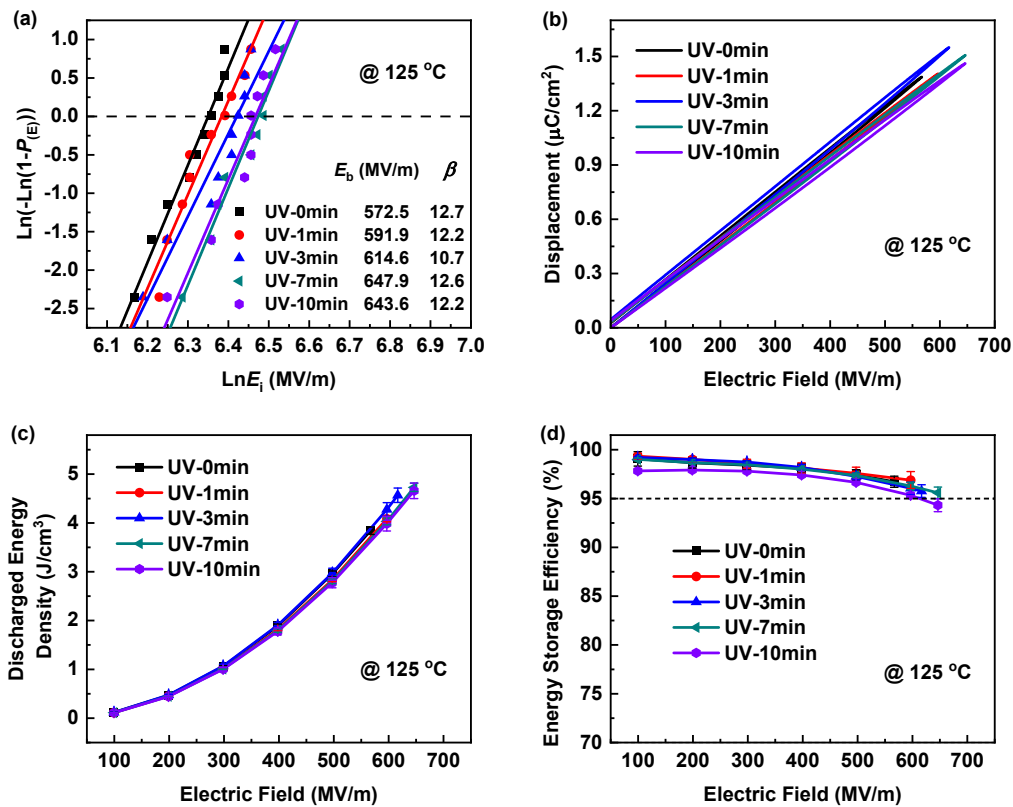**Fig. S9** Energy storage performance of pristine and irradiated COC-6013 films at 125 °C. (a) Weibull distributions of measured breakdown strengths. The solid lines refer to the fitting results using a two-parameter Weibull distribution function. (b) *D-E* curves. (c) Discharged energy density and (d) Energy storage efficiency as a function of electric field. Error bars represent the standard deviations.

**Table S2.** Breakdown strength ($E_b$), discharged energy density ($U_e$), and energy storage efficiency ($\eta$) of pristine and irradiated COC-6013 films at 125 °C.

| Samples | $E_b$ (MV m$^{-1}$) | $U_e$ (J cm$^{-3}$) | $\eta$ @ $E_b$ |
|---------|---------------------|---------------------|-----------------|
| UV-0min | 572.5 | 3.84 | 96.7% |
| UV-1min | 591.9 | 4.08 | 96.9% |
| UV-3min | 614.6 | 4.57 | 95.8% |
| UV-7min | 647.9 | 4.73 | 95.6% |
| UV-10min | 643.6 | 4.66 | 94.3% |

Table S2 summarizes the dielectric energy storage performance of pristine and irradiated COC-6013 films at 125 °C, including breakdown strengths, discharged energy densities, and energy storage efficiencies. The maximum discharged energy density of the UV-7min film is ~4.73 J cm$^{-3}$, which is ~23.2% higher than ~3.84 J cm$^{-3}$ for the pristine film. Of particular importance, all the films have ultra-high energy storage efficiency at the $E_b$.
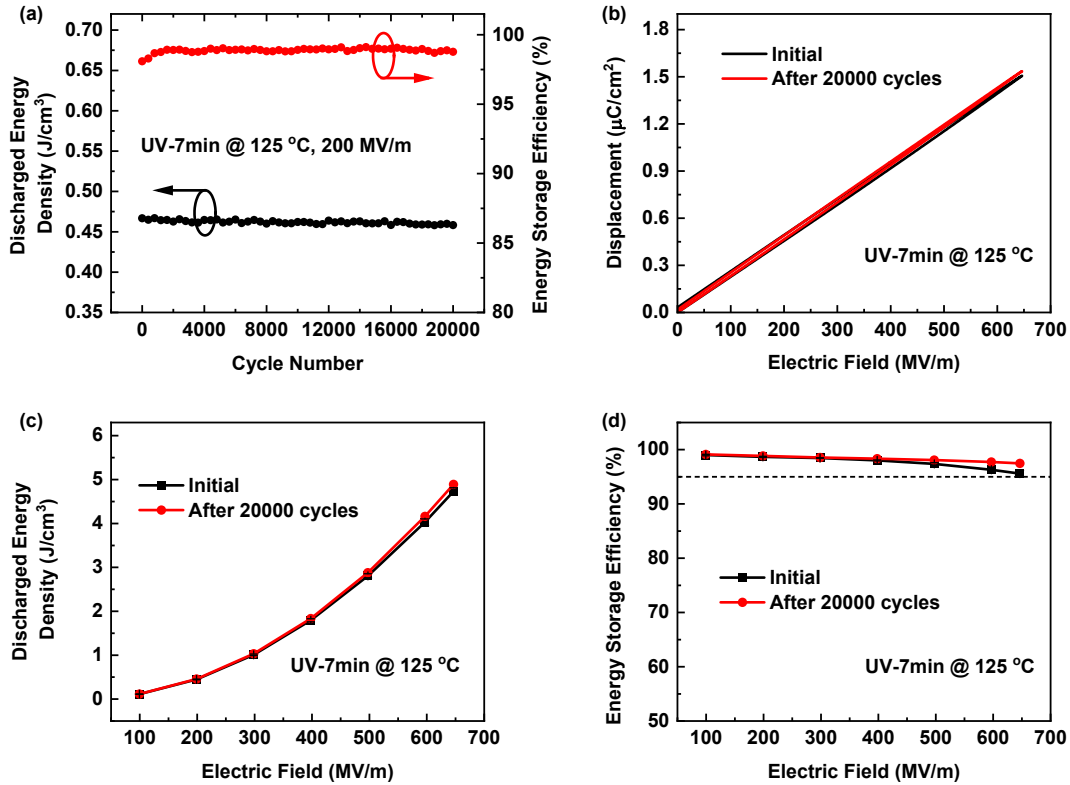


**Fig. S10** (a) Discharged energy density and efficiency as a function of cycle number of UV-7min film measured under 200 MV m$^{-1}$ at 125 °C. (b) *D-E* curves at breakdown strength, (c) Discharged energy density, and (d) Energy storage efficiency as a function of electric field of UV-7min film before and after 20000 cycles tests at 125 °C.

Furthermore, the charge-discharge experiment for UV-7min film was conducted under an electric field of 200 MV m$^{-1}$ (the actual operating electric field in hybrid electric vehicles) at

125 °C, as shown in Fig. S10a. It is obvious that there is no sign of degradation in the discharged energy density and efficiency during 20000 cycles. More importantly, the film after 20000 cycles tests shows no degradation in energy storage performance, including breakdown strength, discharged energy density and efficiency (Fig. S10b-d), demonstrating good dielectric stability of irradiated film. The above results show that our strategy is also effective in improving the energy storage performance of COC film with different contents of norbornene.

## References

1    C. Wu, A. A. Deshmukh, O. Yassin, J. R. Zhou, A. Alamri, J. Vellek, S. Shukla, M. Sotzing, R. Casalini, G. A. Sotzing and Y. Cao, *Proc. Natl. Acad. Sci. U. S. A.*, 2021, **118**, e2115367118.

2    R. R. Lamonte and D. McNally, *Adv. Mater. Processes*, 2001, **159**, 33-36.

3    A. A. Deshmukh, C. Wu, O. Yassin, A. Mishra, L. H. Chen, A. Alamri, Z. Z. Li, J. R. Zhou, Z. Mutlu, M. Sotzing, P. Rajak, S. Shukla, J. Vellek, M. A. Baferani, M. Cakmak, P. Vashishta, R. Ramprasad, Y. Cao and G. Sotzing, *Energy Environ. Sci.*, 2022, **15**, 1307-1314.

4    C. Wu, A. A. Deshmukh, Z. Z. Li, L. H. Chen, A. Alamri, Y. F. Wang, R. Ramprasad, G. A. Sotzing and Y. Cao, *Adv. Mater.*, 2020, **32**, 2000499.

5    A. Gopanna, R. N. Mandapati, S. P. Thomas, K. Rajan and M. Chavali, *Polym. Bull.*, 2019, **76**, 4259-4274.

6    A. Gopanna, S. P. Thomas, K. P. Rajan, R. Rajan, E. Rainosalo, J. Zavašnik and M. Chavali, *Eur. Polym. J.*, 2018, **108**, 439-451.

7    P. J. Wang, Y. Guo, D. Zhou, D. Li, L. X. Pang, W. F. Liu, J. Z. Su, Z. Q. Shi and S. K. Sun, *Adv. Funct. Mater.*, 2022, **32**, 2204155.

8    C. Wu, A. A. Deshmukh, Z. Z. Li, L. H. Chen, A. Alamri, Y. F. Wang, J. R. Zhou, O. Yassin, R. Ramprasad, G. A. Sotzing and Y. Cao, *IEEE Trans. Dielectr. Electr. Insul.*, 2021, **28**, 1468-1470.

9    H. M. Qin, M. Liu, Z. W. Li, Y. H. Fu, J. H. Song, J. Xie, C. X. Xiong and S. Wang, *J. Energy Storage*, 2022, **55**, 105756.

10   Y. P. Pu, W. Wang, X. Guo, R. K. Shi, M. D. Yang and J. W. Li, *J. Mater. Chem. C*, 2019, **7**, 14384-14393.

11   H. Li, D. Ai, L. L. Ren, B. Yao, Z. B. Han, Z. H. Shen, J. J. Wang, L. Q. Chen and Q. Wang, *Adv. Mater.*, 2019, **31**, 1900875.

12   Y. Sun, S. A. Boggs and R. Ramprasad, *Appl. Phys. Lett.*, 2012, **101**, 132906.

13　C. Kim, G. Pilania and R. Ramprasad, *J. Phys. Chem. C*, 2016, **120**, 14575-14580.

14　S. Cheng, Y. Zhou, J. Hu, J. L. He and Q. Li, *IEEE Trans. Dielectr. Electr. Insul.*, 2020, **27**, 498-503.

15　Y. F. Wang, Z. Z. Li, C. Wu, P. N. Zhou, J. R. Zhou, J. D. Huo, K. Davis, A. C. Konstantinou, H. Nguyen and Y. Cao, *Chem. Eng. J.*, 2022, **437**, 135430.

16　K. Y. Zhang, Z. Y. Ma, H. Deng and Q. Fu, *Adv. Compos. Hybrid Mater.*, 2022, **5**, 238-249.

17　A. Kahouli, O. Gallot-Lavallée, P. Rain, O. Lesaint, C. Guillermin and J.-M. Lupin, *IEEE International Conference on Solid Dielectrics*, Bologna, Italy, 2013, 1068-1071.

18　B. Wouters, J. De Vos, G. Desmet, H. Terryn, P. J. Schoenmakers and S. Eeltink, *J. Sep. Sci.*, 2015, **38**, 1123-1129.

19　S. A. Sbeih and A. M. Zihlif, *J. Phys. D: Appl. Phys.*, 2009, **42**, 145405.

20　S. R. Kim and D. J. Kim, *J. Appl. Polym. Sci.*, 2008, **109**, 3439-3446.

21　C. B. B. Luna, D. D. Siqueira, E. S. B. Ferreira, W. A. Silva, J. A. S. Nogueira and E. M. Araújo, *Sustainability*, 2020, **12**, 5272.

22　A. Rahate, K. Nemade and S. Waghuley, *Proceedings of the International Conference on Recent Trends in Applied Physics and Material Science (RAM)*, Bikaner, India, 2013, 809-810.

23　B. Vieille, J. Aucher and L. Taleb, *Mater. Sci. Eng. A*, 2009, **517**, 51-60.

24　S.-W. Kuo and H.-T. Tsai, *Macromolecules*, 2009, **42**, 4701-4711.

25　M. T. Patil, S. N. Lakshminarasimhan and G. Santhosh, *Mater. Today: Proc.*, 2021, **46**, 2564-2571.

26　R. Mishra, S. P. Tripathy, D. Sinha, K. K. Dwivedi, S. Ghosh, D. T. Khathing, M. Müller, D. Fink and W. H. Chung, *Nucl. Instrum. Methods B*, 2000, **168**, 59-64.

27　A. M. A. Reheem, M. I. A. A. Maksoud and A. H. Ashour, *Radiat. Phys. Chem.*, 2016, **125**, 171-175.

28　A. K. Mishra, S. Allauddin, R. Narayan, T. M. Aminabhavi and K. V. S. N. Raju, *Ceram. Int.*, 2012, **38**, 929-934.

29　Z. Wang, M. R. Fang, H. J. Li, Y. F. Wen, C. Wang and Y. P. Pu, *Composites Sci. Technol.*, 2015, **117**, 410-416.

30　A. Torabi, S. H. Jafari, H. A. Khonakdar, V. Goodarzi, L. Y. Yu, V. Altstädt and A. L. Skov, *J. Polym. Res.*, 2022, **29**, 425.

31　V. Mylläri, T.-P. Ruoko and P. Järvelä, *Polym. Degrad. Stab.*, 2014, **109**, 278-284.

32　C. M. Zhang, C. Z. Man, W. W. Wang, L. Jiang and Y. Dan, *Polym. Plast. Technol. Eng.*,

2011, **50**, 810-817.

33    J. Jin, S. J. Chen and J. Zhang, *Polym. Degrad. Stab.*, 2010, **95**, 725-732.

34    X.-L. Shi, M.-S. Cao, X.-Y. Fang, J. Yuan, Y.-Q. Kang and W.-L. Song, *Appl. Phys. Lett.*, 2008, **93**, 223112.

35    R. V. Shinde and A. C. Kumbharkhane, *Appl. Innov. Res.*, 2020, **2**, 167-170.

36    P.-L. Shiao, J.-H. Yang, Y.-S. Chou, M.-C. Lai and Y.-D. Lee, *Mater. Chem. Phys.*, 2013, **141**, 694-704.

37    P. Pal, M. K. Kundu, A. Malas and C. K. Das, *Polym. Compos.*, 2015, **36**, 955-960.

38    R. Ding, C. X. Xu, B. X. Gu, Z. L. Shi, H. T. Wang, L. Ba and Z. D. Xiao, *J. Mater. Sci. Technol.*, 2010, **26**, 601-604.

39    Z.-H. Shen, J.-J. Wang, J.-Y. Jiang, S. X. Huang, Y.-H. Lin, C.-W. Nan, L.-Q. Chen and Y. Shen, *Nat. Commun.*, 2019, **10**, 1843.

40    Z.-H. Shen, J.-J. Wang, J.-Y. Jiang, Y.-H. Lin, C.-W. Nan, L.-Q. Chen and Y. Shen, *Adv. Energy Mater.*, 2018, **8**, 1800509.

41    P. W. Leech, *Mater. Des.*, 2010, **31**, 4858-4861.

42    J. Y. Chen, B. W. Li, Y. Sun, P. X. Zhang, Z. H. Shen, X. Zhang, C. W. Nan and S. J. Zhang, *IET Nanodielectr.*, 2021, **4**, 223-228.

43    H. X. Liu, B.-W. Li, J. Y. Chen, Z. H. Shen, X. Zhang, J. Wang and C.-W. Nan, *ACS Omega*, 2022, **7**, 25999-26004.

44    J. Hu, X. C. Zhao, J. H. Xie, Y. Liu and S. L. Sun, *Polym. Eng. Sci.*, 2022, **62**, 1756-1763.

45    M. H. Gutiérrez-Villarreal and S. A. Zavala-Betancourt, *Int. J. Polym. Sci.*, 2017, **2017**, 1870814.

46    W. S. R. Lago, C. Aymes-Chodur, A. P. Ahoussou and N. Yagoubi, *J. Mater. Sci.*, 2017, **52**, 6879-6904.